Sensors and Materials, Vol. 37, No. 7 (2025) 2989–3003
MYU Tokyo

S & M 4098

Scheduling Optimization of Integrated Energy System Based on Electric-hydrogen Coupling Mechanism

Lingling Li,[1,2] Xinrui Du,[1,2] Hsiung-Cheng Lin,[3*] and Liyuan Zhao[1,2]

[1]State Key Laboratory of Intelligent Power Distribution Equipment and System, Hebei University of Technology, Tianjin 300401, China
[2]Key Laboratory of Electromagnetic Field and Electrical Apparatus Reliability of Hebei Province, Hebei University of Technology, Tianjin 300401, China
[3]Department of Electronic Engineering, National Chin-Yi University of Technology, Taichung 41170, Taiwan

(Received April 28, 2025; accepted May 22, 2025)

Keywords: integrated energy system, sensor, operation optimization, electric-hydrogen coupling, information collection and processing

The synergistic integration of renewable energy generation with an integrated energy system (IES) can potentially reduce carbon emission and thus improve energy efficiency. On the basis of this principle, an electric-hydrogen-coupled integrated energy system (EHC-IES) is proposed, integrating renewable energy generation, an electric-hydrogen conversion device, multi-energy storage, and an intelligent sensing system. A multi-dimensional sensing network is erected to collect real-time wind and solar power generation, energy storage status, and load fluctuation data. It can dynamically adjust the energy supply strategy and realize the adaptive synergistic matching of energy supply and demand sides. An optimization model is established considering the cost of superior-level energy dispatch and the cost of renewable energy disposal penalty, and the enhanced whale optimization algorithm is designed for dispatch optimization. Comparative analysis using multiple scenarios verifies that the electric-hydrogen coupling mechanism can reduce the system operating cost by 25.8 and 17.02% compared with those of the conventional integrated energy system and power-to-gas IES (P2G-IES), respectively, confirming significant economic benefit.

1. Introduction

China has put forward the strategic goals of carbon peaking in 2030 and carbon neutrality in 2060 against the background of accelerated green and low-carbon transformation of the global energy structure.(1) Under this strategic direction, promoting the in-depth cross-border integration of energy technology and information technology and constructing an integrated energy system (IES) with multi-energy flow synergies and distributed adaptive capabilities have become the core paths to drive energy system change.(2) On the basis of this, the coupled system integrating hydrogen production from electricity, hydrogen power generation, and thermal energy gradient utilization effectively breaks the technical bottleneck of renewable energy

*Corresponding author: e-mail: hclin@ncut.edu.tw
https://doi.org/10.18494/SAM5712

ISSN 0914-4935

consumption by breaking the traditional energy barriers. It provides a dynamic balancing mechanism for a high proportion of renewable energy to be connected to the grid.[3]

New energy supply systems, represented by wind and photovoltaic power, have been deeply integrated into comprehensive energy systems with the continuous breakthrough of renewable energy technologies.[4] However, owing to the stochastic nature of power output caused by meteorological dependence, power fluctuation and time-period imbalance between supply and demand still cause significant bottlenecks in renewable energy consumption.[5] Schrotenboer *et al*.[6] constructed a Markov decision model for a wind energy-hydrogen storage coupled system, innovatively quantifying the multi-scenario synergistic optimization strategy of green hydrogen in power peaking, industrial energy supply, and fuel supply, which provides a dynamic decision-making framework for highly volatile renewable energy consumption. Lu *et al*.[7] proposed a stochastic optimization framework for a coupled system based on the probabilistic prediction of photovoltaic output, establishing the dynamic coupling mechanism of electricity-heat-hydrogen with the multi-scenario co-scheduling model. Mao *et al*.[8] established a mixed-integer planning model and a multi-objective decision-making mechanism for the coupled electricity-gas-heat system, providing an economic-environmental two-dimensional optimization path for renewable energy consumption. Tipan-Salazar *et al*.[9] proposed a mixed integer nonlinear programming synergistic optimization model for renewable energy-pumped storage-electrolysis hydrogen production to maximize the system's profit while meeting the weekly green hydrogen demand.

Many scholars use meta-heuristic algorithms to optimize IES. For example, Kumar *et al*.[10] constructed a climate adaptive model by optimizing feature selection through the dragonfly-firefly algorithm to achieve the accurate multi-scenario prediction of power generation. Liu *et al*.[11] proposed a comprehensive district energy system integrating electrolytic hydrogen production carbon capture and waste heat recovery, which is solved by a non-dominated sequential genetic algorithm to improve the efficiency of comprehensive energy utilization significantly. Cao *et al*.[12] broke through the bottleneck of traditional heat network models in high-dimensional nonlinear parameter identification through a multi-objective genetic optimization algorithm. Li *et al*.[13] proposed a forbidden search augmented hybrid crow algorithm to resolve time-varying tariff-charging queuing coupling constraints, breaking through the paradigm of independent optimization research on cold chain and electric paths. Gao *et al*.[14] developed a power storage-heat storage cooperative control strategy using an improved multi-objective particle swarm algorithm to effectively solve the fluctuation adaptation problem in a multi-energy flow coupled system.

In this study, we propose an electric-hydrogen-coupled integrated energy system (EHC-IES) to construct a temporally and spatially decoupled multi-energy flow network through the closed-loop architecture of wind power generation, electrolysis hydrogen production, and hydrogen storage and peaking. The rest of this study is structured as follows. Section 2 presents the system structure and optimization model of EHC-IES. The strategy of the enhanced whale optimization algorithm (EWOA) algorithm is described in Sect. 3. As discussed in Sect. 4, we conducted a scenario analysis to validate the effectiveness of the EHC-IES and EWOA algorithms. Conclusions and perspectives are summarized in Sect. 5.

2. System Model

2.1 System structure

The EHC-IES architecture proposed in this study is shown in Fig. 1. The wind turbine (WT) and photovoltaic (PV) complementary generation architecture is used on the generation side. At the energy conversion layer, the electric-hydrogen coupling mechanism is adopted. The electric hydrogen plant (EHP) has a multi-physics sensor array to monitor key parameters such as electrolysis current, voltage, hydrogen yield, and plant temperature to convert surplus electrical energy into hydrogen energy. Some hydrogen and carbon dioxide are synthesized into natural gas in the methane reactor (MR). The pressure sensor deployed in MR continuously collects the CO_2/H_2 gas mixture ratio data to realize the efficient preparation of natural gas. The generated natural gas is supplied to the combined heat and power plant (CHP) and gas boiler (GB) to form a carbon-closed loop. The hydrogen fuel cell (HFC) directly converts the remaining hydrogen to realize the short-chain conversion of "electricity-hydrogen-electricity/heat". The short-chain conversion reduces energy loss compared with the traditional long-chain path of "electricity-

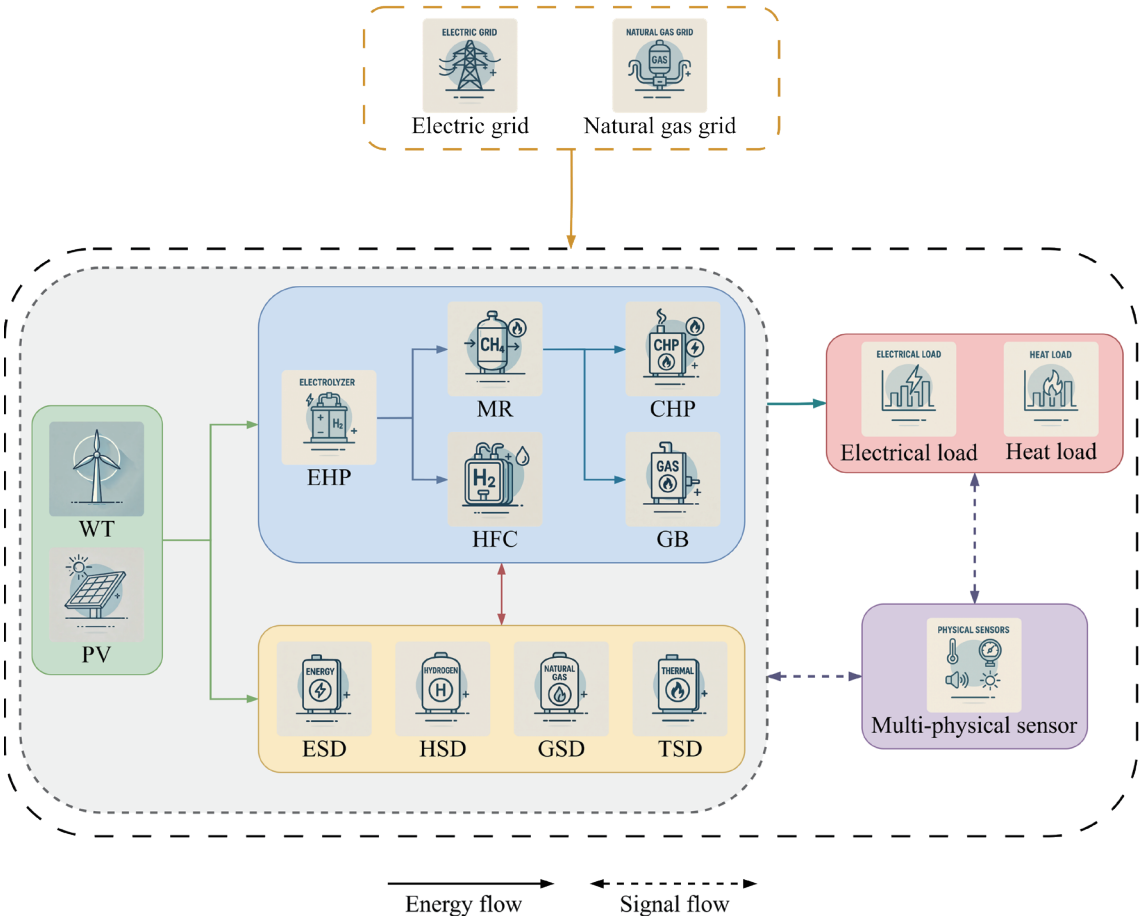

Fig. 1. (Color online) EHC-IES architecture.

hydrogen-methane-electricity/heat". The energy storage system adopts a multi-configuration model, with the electric energy storage device (ESD) and thermal energy storage device (TSD) constituting the electric-thermal buffer layer and the hydrogen energy storage device (HSD) and gas energy storage device (GSD) realizing the staggered adjustment of gas fuel. The intelligent sensing system captures the fluctuation characteristics of thermal and electrical loads in real time through temperature and electrical energy sensors.

2.2 Optimization model

2.2.1 Objective function

We constructed the total operating cost target C by considering the cost of the superior-level energy dispatch and the cost of the renewable energy disposal penalty of EHC-IES.

$$C = \min\left(c_{grid} + c_{waste}\right) \tag{1}$$

$$c_{grid} = \sum_{t=1}^{T} r_e^{grid}(t) E_e^{grid}(t) + \sum_{t=1}^{T} r_g^{grid}(t) E_g^{grid}(t) \tag{2}$$

$$c_{waste} = \alpha^{WT} \sum_{t=1}^{T} E_{waste}^{WT}(t) + \alpha^{PV} \sum_{t=1}^{T} E_{waste}^{PV}(t) \tag{3}$$

Here, r_e^{grid} and r_g^{grid} are the prices of electricity and natural gas from the superior energy source in time period t, $E_e^{grid}(t)$ and $E_g^{grid}(t)$ are the electricity and natural gas power dispatched from the superior energy source in time period t, α^{WT} and α^{PV} are the penalty cost coefficients per unit of discarded power of WT and PV, and $E_{waste}^{WT}(t)$ and $E_{waste}^{PV}(t)$ are the WT discarded power and PV discarded power in time period t, respectively.

2.2.2 Constraints

During operation, EHC-IES must reach a dynamic equilibrium constraint on the multi-energy complementarity of electricity, heat, hydrogen, and natural gas.

$$E_e^{grid}(t) + E_e^{WT}(t) + E_e^{PV}(t) + E_e^{HFC}(t) + E_e^{CHP}(t) + E_e^{ESD}(t) = E_{load}^{e}(t) + E_{EHP}^{e}(t) \tag{4}$$

$$E_h^{HFC}(t) + E_h^{CHP}(t) + E_h^{GB}(t) + E_h^{TSD}(t) = E_{load}^{h}(t) \tag{5}$$

$$E_{H_2}^{EHP}(t) + E_{H_2}^{HSD}(t) = E_{HFC}^{H_2}(t) \tag{6}$$

$$E_g^{gird}(t) + E_g^{MR}(t) + E_g^{GSD}(t) = E_g^{CHP}(t) + E_g^{GB}(t) \tag{7}$$

Here, $E_e^{HFC}(t)$ and $E_h^{HFC}(t)$ are the electrical and thermal outputs of HFC in time period t, respectively. $E_e^{CHP}(t)$ and $E_h^{CHP}(t)$ are the electrical and thermal outputs of CHP in time period t, respectively. $E_{EHP}^{e}(t)$ is the electrical consumption of EHP in time period t, $E_h^{GB}(t)$ is the thermal output of GB in time period t, and $E_{H_2}^{EHP}(t)$ is the hydrogen output of EHP in time period t. $E_e^{ESD}(t)$, $E_h^{TSD}(t)$, $E_{H_2}^{HSD}(t)$, and $E_g^{GSD}(t)$ are the energy outputs of the electrical, thermal, hydrogen, and natural gas storage devices in time period t. $E_{load}^{e}(t)$ and $E_{load}^{h}(t)$ are the electrical and thermal loads in time period t, respectively. $E_{HFC}^{H_2}(t)$ is the hydrogen consumption of HFC in time period t, $E_g^{MR}(t)$ is the natural gas output of MR in time period t, and $E_{CHP}^{g}(t)$ and $E_{GB}^{g}(t)$ are the natural gas consumption of CHP and GB in time period t, respectively.

3. Optimization Method

The optimal scheduling of EHC-IES is a multi-coupled constrained optimization problem, and the meta-heuristic algorithm based on the global-local balanced search mechanism demonstrates significant advantages in solving such optimization problems. Although the whale optimization algorithm (WOA) inspired by the hunting behavior of the whale group exhibits good spatial exploration characteristics, it is prone to the premature convergence phenomenon in the dynamic optimization search process.[15] On the basis of this principle, the strategy of EWOA is proposed in this study as follows.

3.1 Convergence regulation factor

A convergence regulation factor v is introduced to better utilize the nonlinear property in the global search and local exploitation capabilities.

$$v = 2 - 2\sin(\zeta \frac{t}{max_{iter}} \pi + \psi) \tag{8}$$

Here, max_{iter} is the maximum number of iterations, t is the current number of iterations, and ζ and ψ are the relevant parameters ($\zeta = 0.5$, $\psi = 0$).

3.2 Dynamic balance weighting strategy and multidirectional perturbation evolutionary strategy

Dynamically balanced weighting and multidirectional perturbation evolution strategies are established. They can overcome the problems of insufficient development capability and degradation of solution quality in the deep optimization phase of WOA.

The dynamic balance weighting function is expressed as

$$\kappa = 1 - \frac{e^{\frac{t}{max_{iter}}} - 1}{e - 1}, \tag{9}$$

$$P(t+1) = \kappa P_x(t). \tag{10}$$

Here, κ is the dynamic balance weighting factor and $P_x(t)$ is the current optimal solution.

The multidirectional perturbation evolutionary strategy is as follows:

$$P(t+1) = k_1(P_x(t) - P(t)) + k_2(P'(t) - P(t)). \tag{11}$$

Here, k_1 and k_2 are random numbers in [0, 1]; $P'(t)$ is a random individual in the population.

The individual evolutionary path is divided into three stages: focused exploitation, spatial expansion, and random sampling. A dynamically balanced weight strategy updates the position when an individual carries out focused development or spatial expansion. Then, the individual updates the position through a multi-way perturbation evolutionary strategy. The historical optimal position is selected by integrating the optimal solution information before and after updating. The synergy of the dual strategies significantly improves convergence efficiency and suppresses the premature convergence phenomenon, which enhances the algorithm's global exploration ability.

The flowchart of EWOA is shown in Fig. 2.

4. Case Analysis

4.1 Basic data

The effectiveness of the proposed economic dispatch optimization model using EWOA is analyzed by setting up an experimental example using a daily operation scenario. The superior energy price signals,[16] the operating parameters of each unit, and the configuration parameters of each storage device are shown in Tables 1–3, respectively.[17]

Table 1 shows that EHC-IES is affected by the time-sharing tariff mechanism, with significant differences in electricity prices during peak and valley hours, while the natural gas market price exhibits smooth fluctuation throughout the day. Table 2 shows that all types of energy device are configured with 20% power creep constraints, which not only constrains the instantaneous power regulation capability of the devices but also effectively avoids the problem of frequent start-stop during operation. Table 3 shows that the energy storage system adopts a dual safety strategy, setting 10–90% operation constraints in the capacity dimension to reserve safety margins while simultaneously imposing a 20% ramp rate constraint in the power dimension, which guarantees the system's dynamic regulating capability and realizes the safety of the equipment.

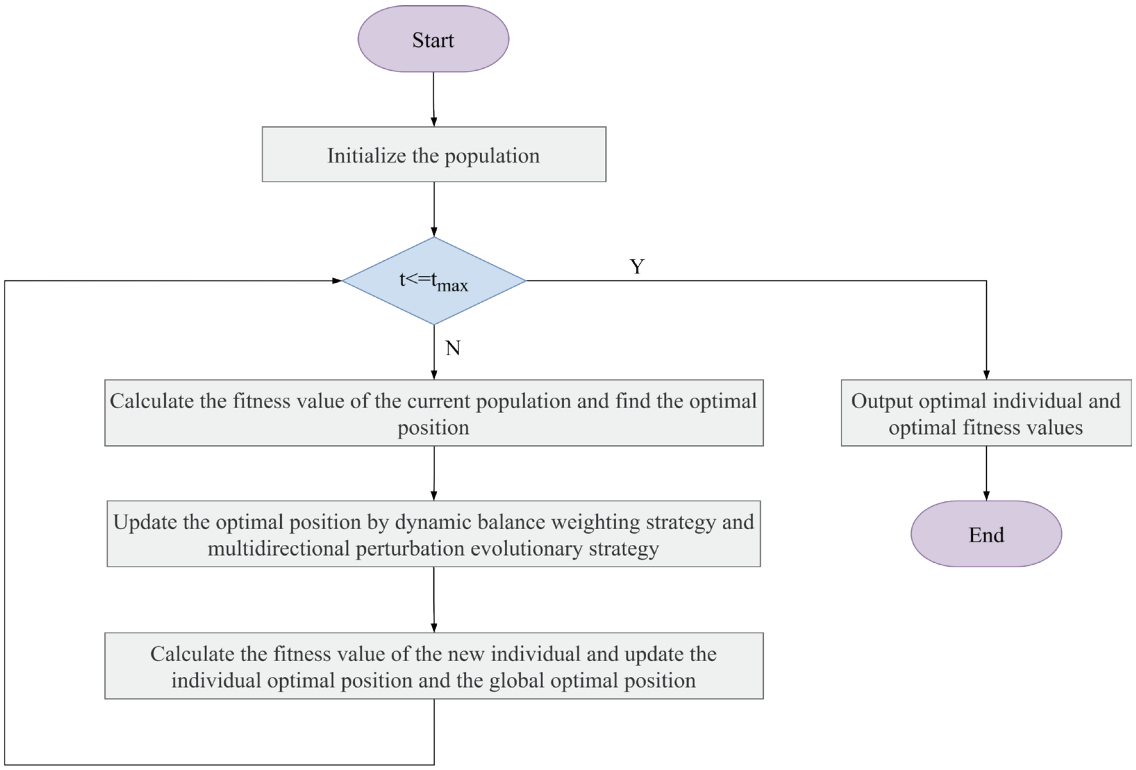

Fig. 2. (Color online) Flowchart of EWOA.

Table 1
Market electricity and natural gas price signals.

Items	Time interval	Price
Electricity price	1:00–4:00, 21:00–24:00	0.43
	5:00–8:00, 17:00–20:00	0.90
	9:00–16:00	1.15
Natural gas price	1:00–24:00	0.35

Table 2
Unit equipment operating parameters.

Items	EHP	MR	HFC	CHP	GB
Capacity (kW)	850	450	380	380	800
Energy conversion efficiency (%)	90	95	90	92	95
Climbing constraint (%)	20	20	20	20	20

Table 3
Energy storage equipment operating parameters.

Items	ESD	TSD	HSD	GSD
Capacity (kW)	500	350	450	400
Capacity upper bound (%)	90	90	90	90
Capacity lower bound (%)	10	10	10	10
Climbing constraint (%)	20	20	20	20

4.2 Performance test and analysis

The F11–F16 test functions in the CEC test set are selected for evaluation in this study. The population size is N_{pop} = 80, and the corresponding function convergence trajectories and solution space distributions are shown in Fig. 3. Here, the polar lights optimization algorithm (PLO),[18] crown porcupine optimization algorithm (CPO),[19] and WOA were selected for comparison in this study. The number of algorithm evolutions is set to 4000, the population size is the same as that of EWOA, and each algorithm is repeated 70 times. The performance results are shown in Tables 4 and 5.

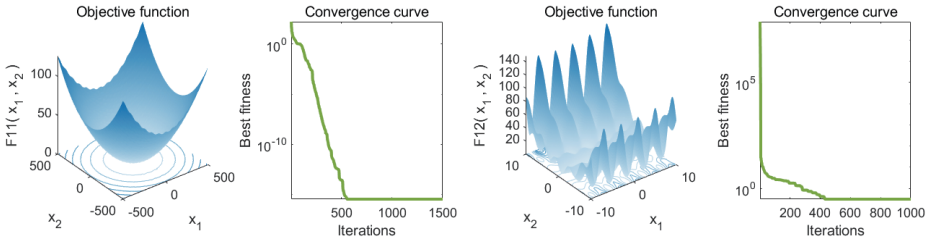

(a) $$F11 = \frac{1}{4000}\sum_{i=1}^{n} x_i^2 - \prod_{i=1}^{n}\cos\left(\frac{x_i}{\sqrt{i}}\right) + 1$$

(b) $$F12 = \begin{cases} 100(x_i - 10)^4 & x_i > 10 \\ 0 & -10 \le x_i \le 10 \\ 100(-x_i - 10)^4 & x_i < -10 \end{cases}.$$

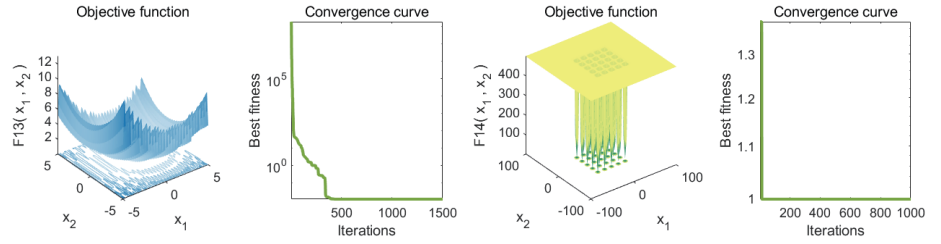

(c) $$F13 = 0.1\begin{bmatrix} \sin^2(3\pi x_1) \\ +\sum_{i=1}^{d-1}(x_i - 1)^2(1 + \sin^2(3\pi x_{i+1})) \\ +(x_d - 1)^2(1 + \sin^2(2\pi x_d)) \end{bmatrix}$$

(d) $$F14 = \frac{1}{\frac{1}{500} + \sum_{j=1}^{25}\frac{1}{j + ((x_1 - a_{1j})^6 + (x_2 - a_{2j})^6)}}$$

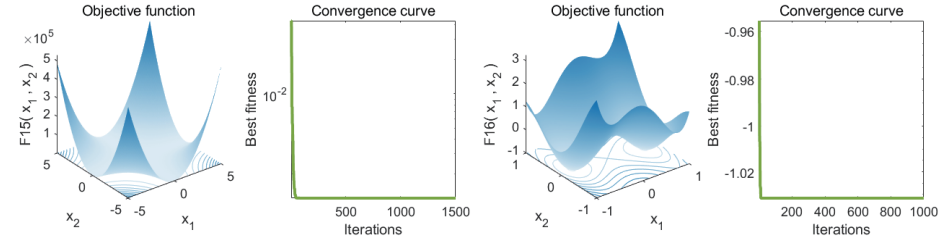

(e) $$F15 = \min_x \sum_{k=1}^{11}\left[a_k - \frac{x_1(b_k^2 + x_2 b_k)}{b_k^2 + x_3 b_k + x_4}\right]^2$$

(f) $$F16 = 4x_1^2 - 2.1x_1^4 + \frac{x_1^6}{3} + x_1 x_2 - 4x_2^2 + 4x_2^4$$

Fig. 3. EWOA test under F11–F16.

Table 4
Mean value (standard deviation) of test results under different algorithms.

Function	EWOA	WOA	PLO	CPO
$F1=\sum_{i=1}^{n}x_i^2$	4.6607e+3 (4.53e+3)	4.4926e+5 (2.79e+5)	3.2649e+10 (1.53e+10)	1.1650e+7 (8.64e+6)
$F2=\sum_{i=1}^{n}\lvert x_i\rvert+\prod_{i=1}^{n}\lvert x_i\rvert$	1.6127e+3 (2.23e+2)	1.5541e+3 (2.22e+2)	2.1069e+3 (3.43e+2)	1.5791e+3 (1.14e+2)
$F3=\sum_{i=1}^{n}\left(\sum_{k=1}^{i}x_k\right)^2$	7.3471e+2 (1.91e+1)	7.1936e+2 (6.29e+0)	1.0504e+3 (1.35e+2)	7.2072e+2 (3.60e+0)
$F4=\max\left(\lvert x_1\rvert,\lvert x_2\rvert,\ldots,\lvert x_n\rvert\right)$	1.9042e+3 (3.32e+0)	1.9017e+3 (7.43e−1)	4.1736e+6 (1.92e+7)	1.9028e+3 (1.24e+0)
$F5=\sum_{i=1}^{d-1}\left[100(x_{i+1}-x_i^2)^2+(x_i-1)^2\right]$	2.5600e+3 (2.26e+3)	4.6767e+3 (3.38e+3)	9.3085e+9 (6.10e+9)	2.8728e+3 (1.07e+3)
$F6=\sum_{i=1}^{n}\left(\lvert x_i+0.5\rvert\right)^2$	1.6934e+3 (1.06e+2)	1.6266e+3 (4.59e+1)	1.9552e+3 (1.93e+2)	1.6125e+3 (9.35e+0)
$F7=\sum_{i=1}^{D}i\cdot x_i^4+\text{ò},\quad \text{ò}\sim U(0,1)$	2.1522e+3 (7.04e+1)	2.1033e+3 (6.57e+0)	2.2794e+3 (1.61e+2)	2.1059e+3 (5.32e+0)
$F8=\sum_{i=1}^{n}\left(-x_i\cdot\sin\left(\sqrt{\lvert x_i\rvert}\right)\right)$	2.5955e+3 (4.09e+2)	2.2438e+3 (4.46e+1)	3.2119e+3 (6.65e+2)	2.2667e+3 (3.69e+1)
$F9=10n+\sum_{i=1}^{n}\left[x_i^2-10\cos(2\pi x_i)\right]$	2.6893e+3 (1.19e+2)	2.5484e+3 (8.68e+1)	2.7339e+3 (1.55e+2)	2.5637e+3 (4.91e+1)
$F10=-20e^{-0.2\sqrt{\frac{1}{n}\sum_{i=1}^{n}x_i^2}}-e^{\frac{1}{n}\sum_{i=1}^{n}\cos(2\pi x_i)}+20+e$	2.8734e+3 (5.68e+1)	2.8479e+3 (1.01e+1)	2.8390e+3 (7.46e+1)	2.8510e+3 (2.31e+0)

Table 5
Runtime of test results under different algorithms.

Function	EWOA	WOA	PLO	CPO
$F1=\sum_{i=1}^{n}x_i^2$	1.90e−02	2.32e−02	1.02e−01	5.83e−02
$F2=\sum_{i=1}^{n}\lvert x_i\rvert+\prod_{i=1}^{n}\lvert x_i\rvert$	1.99e−02	2.28e−02	1.18e−01	5.87e−02
$F3=\sum_{i=1}^{n}\left(\sum_{k=1}^{i}x_k\right)^2$	2.10e−02	2.20e−02	1.12e−01	5.77e−02
$F4=\max\left(\lvert x_1\rvert,\lvert x_2\rvert,\ldots,\lvert x_n\rvert\right)$	1.89e−02	2.24e−02	1.05e−01	5.67e−02
$F5=\sum_{i=1}^{d-1}\left[100(x_{i+1}-x_i^2)^2+(x_i-1)^2\right]$	2.03e−02	2.62e−02	1.37e−01	5.69e−02
$F6=\sum_{i=1}^{n}\left(\lvert x_i+0.5\rvert\right)^2$	2.14e−02	2.61e−02	1.42e−01	6.17e−02
$F7=\sum_{i=1}^{D}i\cdot x_i^4+\text{ò},\quad \text{ò}\sim U(0,1)$	2.07e−02	2.53e−02	1.37e−01	6.03e−02
$F8=\sum_{i=1}^{n}\left(-x_i\cdot\sin\left(\sqrt{\lvert x_i\rvert}\right)\right)$	2.32e−02	2.88e−02	1.81e−01	6.28e−02
$F9=10n+\sum_{i=1}^{n}\left[x_i^2-10\cos(2\pi x_i)\right]$	2.49e−02	3.15e−02	1.86e−01	6.80e−02
$F10=-20e^{-0.2\sqrt{\frac{1}{n}\sum_{i=1}^{n}x_i^2}}-e^{\frac{1}{n}\sum_{i=1}^{n}\cos(2\pi x_i)}+20+e$	2.56e−02	3.06e−02	2.06e−01	6.73e−02

As shown in Fig. 3, the EWOA algorithm exhibits convergence robustness on the 10 benchmark functions containing unimodal, composite, and fixed multimodal modes. Table 4 shows that the algorithm significantly outperforms the control algorithm in terms of global optimal solution search accuracy for 60% of the tested functions in 80 independent experiments. Moreover, by comparison in Table 5, it can be seen that EOWA exhibits outstanding processing power in terms of computational time consumption.

4.3 Case results and analysis

The optimized output state of each equipment used in the proposed algorithm is shown in Figs. 4–9. As shown in Fig. 4, EHC-IES generates redundant power at night when the wind power output peaks and in the daytime when the wind-solar hybrid generation meets the electric load demand, and the excess power needs to be consumed in multiple ways. In this process, EHC-IES prioritizes delivering surplus power to EHP for hydrogen production and simultaneously realizes inter-time regulation through the storage device. As shown in Figs. 5 and 6, EHC-IES delivers the primary hydrogen resources to HFC for cogeneration; part of hydrogen resources is diverted to MR for natural gas synthesis, and the remaining part is stored in HSD as hydrogen for intertemporal regulation. HFC maintains a full-generation state owing to its high energy-efficiency conversion. At the same time, the MR pathway is converted by GB and CHP,

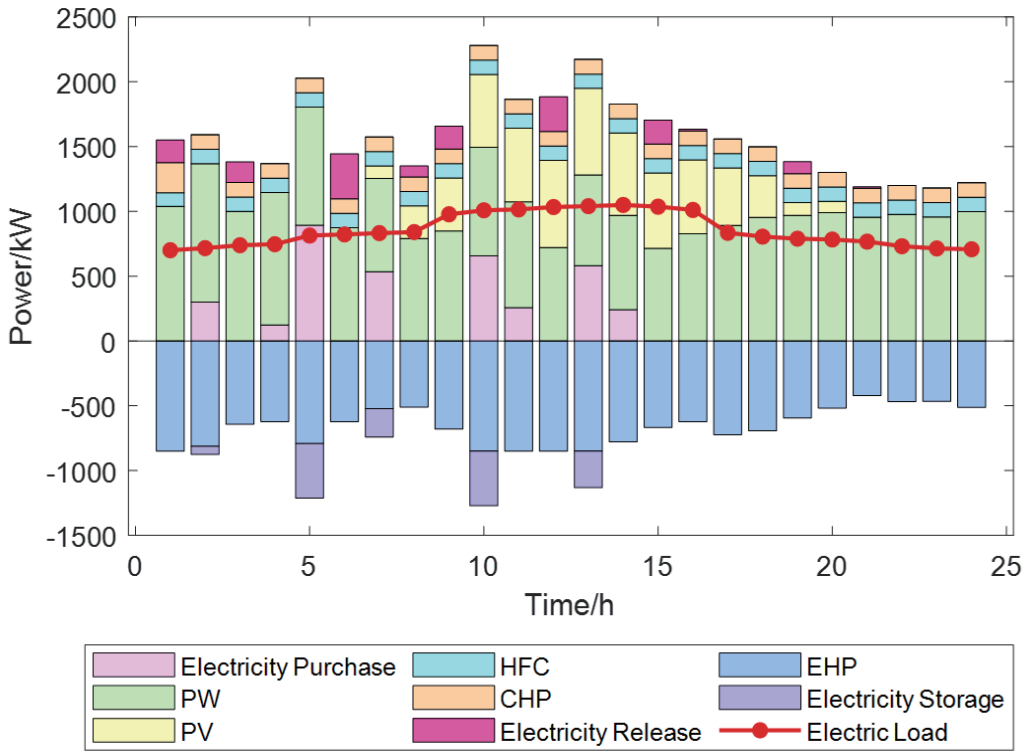

Fig. 4. (Color online) Electric power balance.

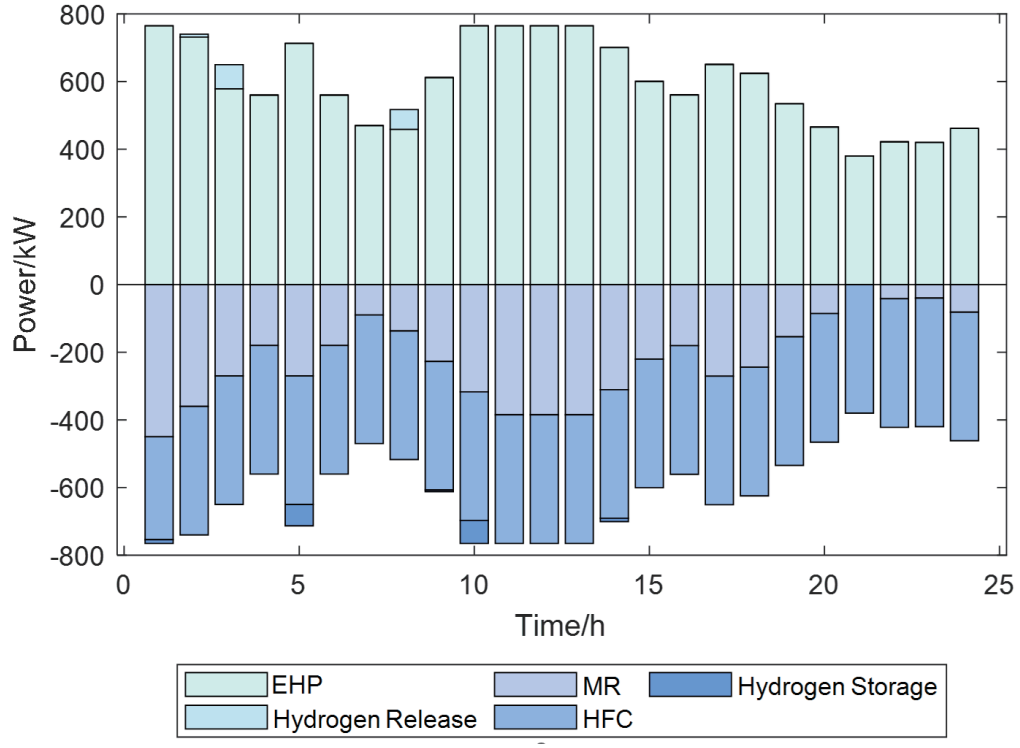

Fig. 5. (Color online) Hydrogen power balance.

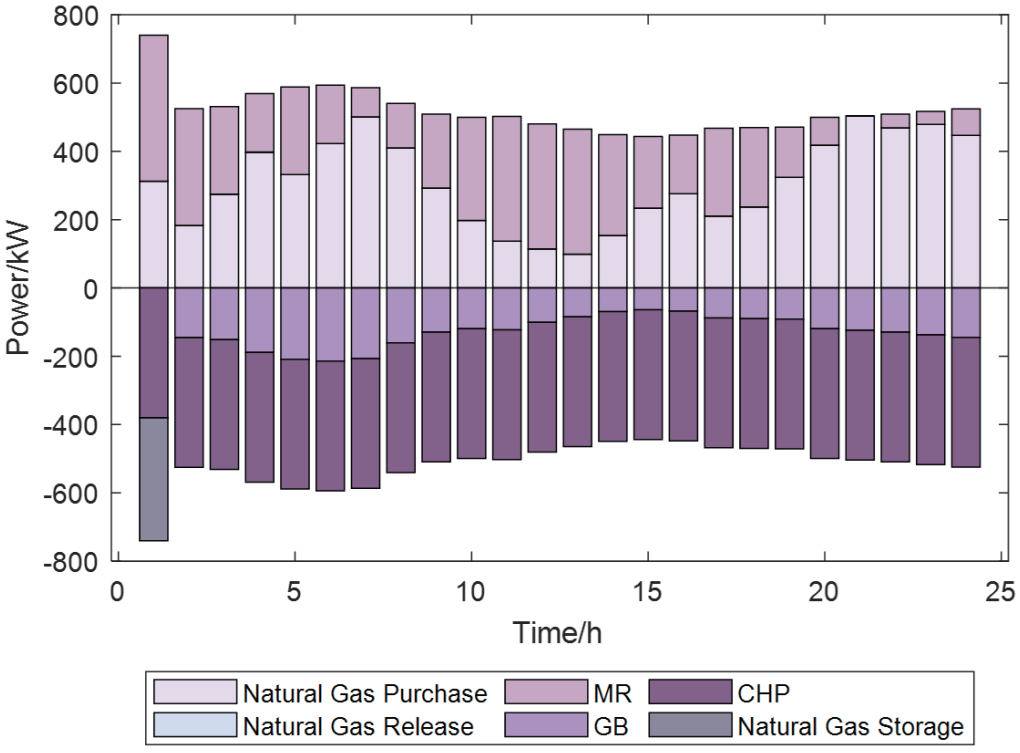

Fig. 6. (Color online) Natural gas power balance.

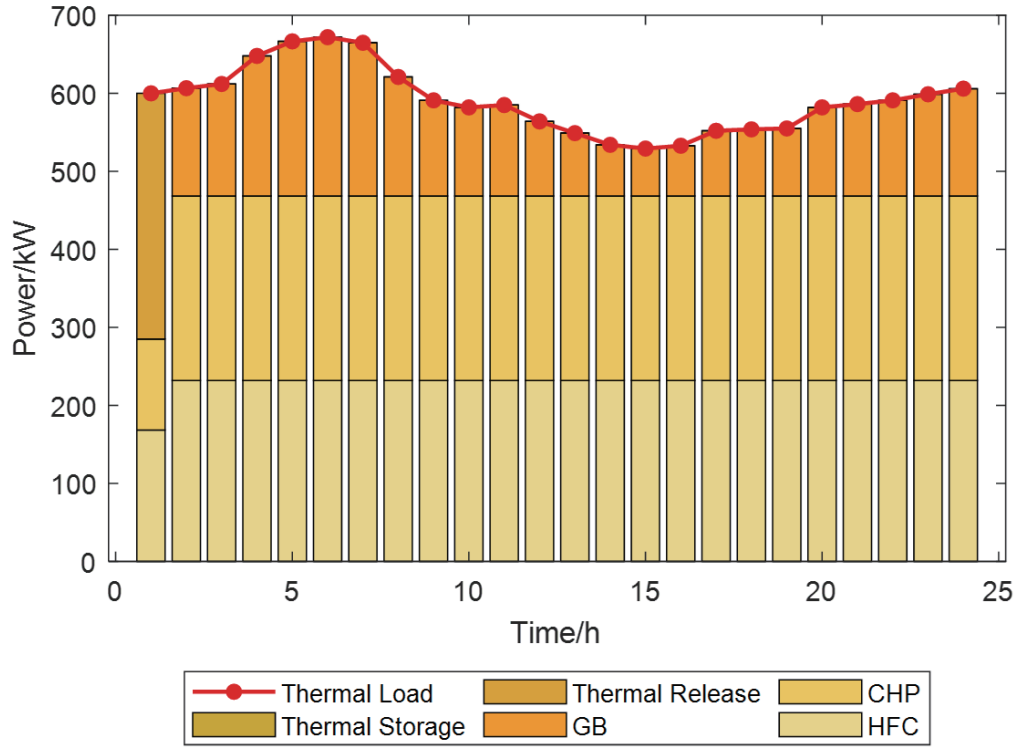

Fig. 7. (Color online) Thermal power balance.

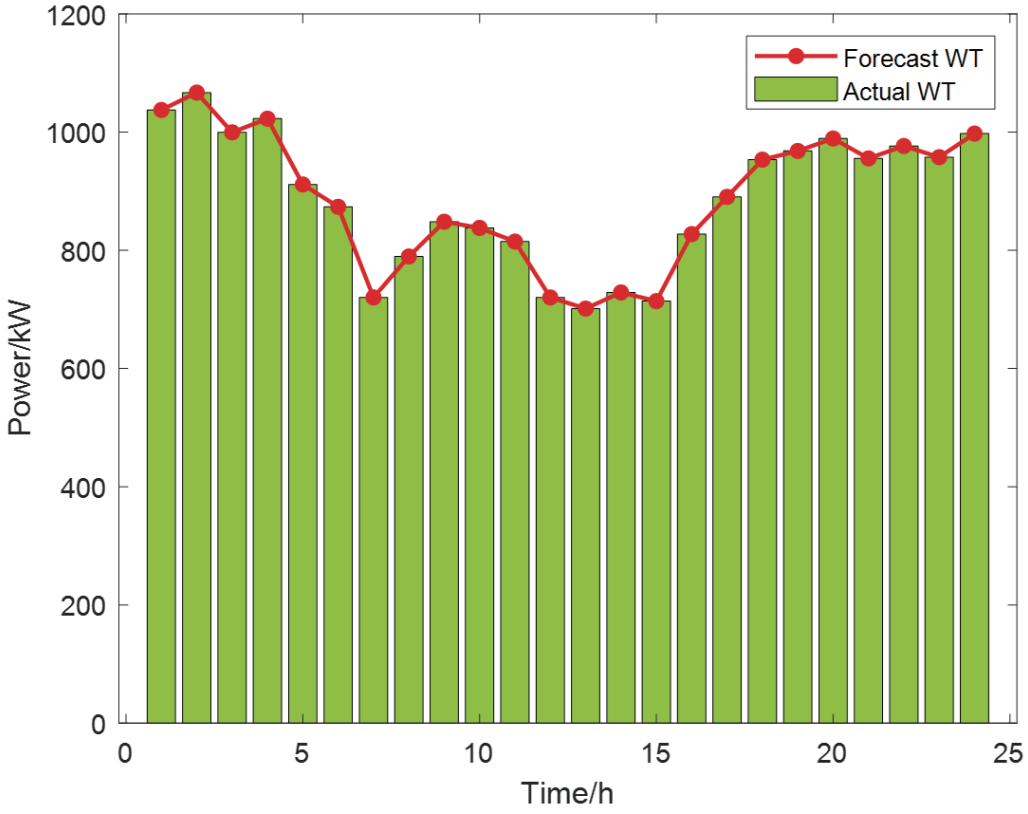

Fig. 8. (Color online) WT balance.

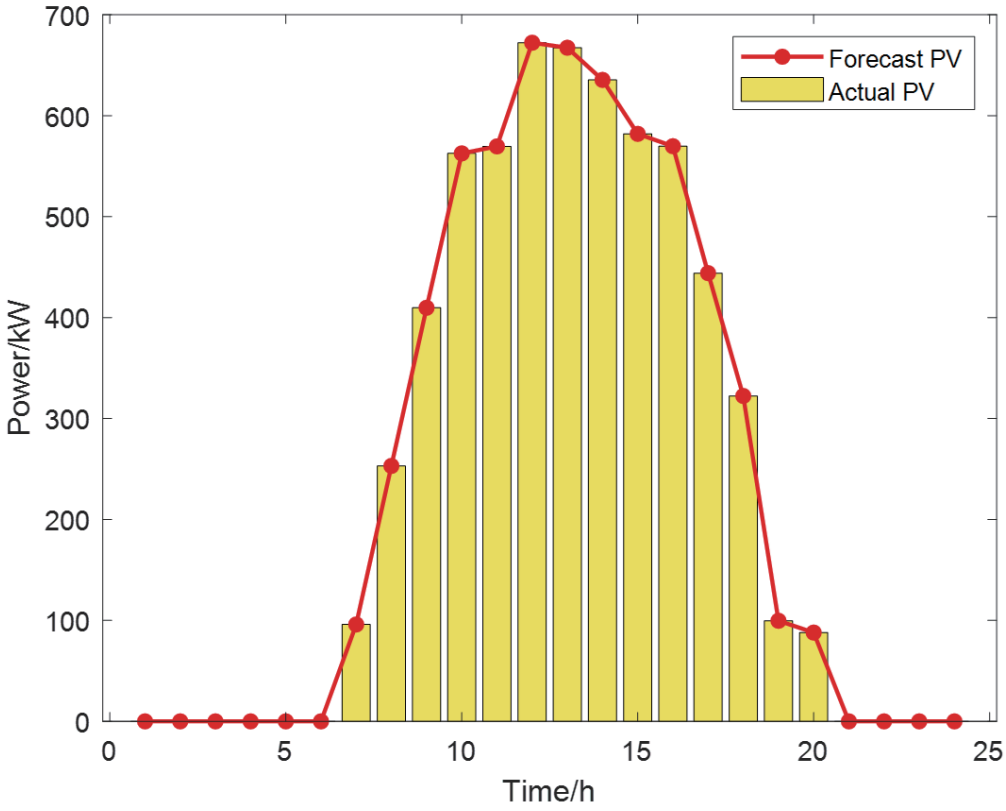

Fig. 9. (Color online) PV balance.

which involves a multi-stage energy attenuation of hydrogen-methane-heat/electricity. Therefore, EHC-IES adopts the optimization strategy of "HFC priority direct supply, MR graded conversion, and hydrogen storage to cut peaks and fill valleys." As shown in Fig. 7, during the peak heat demand period, HFC dominates the thermal energy supply by its zero-carbon emission advantage, and the CHP unit enhances the energy efficiency margin of the system through the synergy of heat and power, while the GB unit makes up for the shortfall. Figures 8 and 9 show that EHC-IES realizes the full WT and PV power consumption. From the above analysis, it can be seen that the EHC-IES constructed in this study can significantly increase the penetration rate of renewable energy and the economic benefits of EHC-IES.

To evaluate the effectiveness of the electric-hydrogen coupling mechanism on IES, four scenarios were set up for the configuration in cost as follows.

Case 1: IES without electric-hydrogen coupling mechanism.

Case 2: IES with traditional P2G mechanism.

Case 3: IES with electric-hydrogen coupling mechanism (i.e., EHC-IES).

Case 4: EHC-IES with WT and PV disturbances.

The optimized scheduling results for the above scenarios are shown in Table 6.

It can be seen that Case 1 without the electric-hydrogen coupling mechanism exhibits an evident energy abandonment phenomenon, i.e., ¥307.70 in energy disposal cost. Case 2 adopts P2G technology to prepare natural gas from redundant electric energy, matching power demand but reducing the expenditure on purchased energy. Case 3 with EHC-IES promises that surplus

Table 6
Benefit comparison in cost.

Items	Case 1	Case 2	Case 3	Case 4
Upper-level electricity dispatch cost (¥)	4341.61	4015.37	3459.19	3983.52
Upper-level natural gas dispatch cost (¥)	3517.47	3285.92	2600.74	3457.48
Renewable energy disposal cost (¥)	307.70	0	0	792.16
Total cost (¥)	8166.78	7301.29	6059.93	8233.16

electric power is made from hydrogen by electrolysis to generate electricity and heat, creating a multistage energy optimization path. Therefore, the operating cost of Case 3 is reduced by ¥2106.85 and ¥1241.36 compared with Cases 1 and 2, respectively. This shows that the electricity-hydrogen coupling mechanism enhances the operating economy and renewable energy consumption capacity through energy gradient conversion.

Case 4 introduces WT and PV perturbations that lead to a dynamic imbalance between power supply and demand, making it difficult for EHC-IES to match volatile power inputs in real time. Although EHP can produce hydrogen, its regulation rate and capacity may not be able to absorb the sudden increase in WT and PV power. Therefore, HSD must frequently switch the hydrogen charging and discharging state under fluctuating scenarios, leading to decreased efficiency. To smooth WT and PV perturbations, EHC-IES is forced to call for high-cost natural gas backup, weakening the advantage of the electric-hydrogen coupling mechanism in peak shaving and valley filling.

5. Conclusions

The EHC-IES proposed in this study constructs a dynamic transmission optimization model for the hydrogen energy medium by deploying a multi-physics sensor array to monitor key parameters such as wind and light outputs, storage equipment pressure, and load fluctuations in real time. On the basis of the multi-source data flow collected by the sensors, the electricity-hydrogen conversion priority is dynamically adjusted to reduce cascade losses. Thus, the penetration rate of renewable energy is significantly increased. Multi-dimensional benchmark tests validate the proposed EWOA and have significant advantages in convergence speed and optimization accuracy. Through a comparative study, EHC-IES reduces the operating cost by 25.8 and 17.02% through electric-hydrogen coupling and energy gradient regulation, respectively, compared with the other two schemes. Subsequent studies can be explored by introducing IES into the multi-energy market for auxiliary service revenue channels. In addition, further study can be focused on the electricity, heat, and natural gas load demand response to break through the existing single flexibility constraint on the equipment side.

Acknowledgments

This study was supported by Project No. 202305B029 and Tianjin Carbon Peak and Carbon Neutrality Technology Major Project (Grant no. 24ZXTKSN00030) and Tianjin Natural Science Foundation Project (Grant no. 23JCQNJC01060).

References

1 J. Zhang and Z. Hu: Energy **322** (2025) 135596. https://doi.org/10.1016/j.energy.2025.135596
2 W. Liang, S. Wang, X. Li, X. Li, and K. Xu: Electr. Power Syst. Res. **243** (2025) 111484. https://doi.org/10.1016/j.epsr.2025.111484
3 J. Duan, Q. Tian, Q. Gao, and Z. Zhou: Energy **323** (2025) 135771. https://doi.org/10.1016/j.energy.2025.135771
4 Y. Li, W. Hu, F. Zhang, and Y. Li: Energy **319** (2025) 135055. https://doi.org/10.1016/j.energy.2025.135055
5 J. Zhang, X. Li, Q. Tan, Z. Zhong, and Q. Zhao: J. Energy Storage **109** (2025) 115109. https://doi.org/10.1016/j.est.2024.115109
6 A. H. Schrotenboer, A. A. T. Veenstra, M. A. J. u. h. Broek, and E. Ursavas: Renewable Sustainable Energy Rev. **168** (2022) 112744. https://doi.org/10.1016/j.rser.2022.112744
7 Z. Lu, Q. Zhu, W. Zhang, and H. Lin: Energy Rep. **9** (2023) https://doi.org/10.1016/j.egyr.2023.01.076
8 Y. Mao, X. Li, J. Liu, M. Yu, M. K. Kim, and K. Yang: Appl. Therm. Eng. **268** (2025) 125942. https://doi.org/10.1016/j.applthermaleng.2025.125942
9 L. Tipan-Salazar, N. Naval, and J. M. Yusta: Renewable Energy **246** (2025) 122939. https://doi.org/10.1016/j.renene.2025.122939
10 S. S. Kumar, A. Karthick, R. Shankar, and G. Dharmaraj: Energy **308** (2024) 132926. https://doi.org/10.1016/j.energy.2024.132926
11 S. Liu, L. Song, T. Wang, Y. Hao, B. Dai, and Z. Wang: Energy Convers. Manage. **291** (2023) 117345. https://doi.org/10.1016/j.enconman.2023.117345
12 X. Cao, Z. Lu, Y. Wang, D. Li, H. Dong, Z. Yan, and C. Liu: Appl. Therm. Eng. **240** (2024) 122290. https://doi.org/10.1016/j.applthermaleng.2023.122290
13 Y. Li, M. K. Lim, W. Xiong, X. Huang, Y. Shi, and S. Wang: Ind. Manage. Date Syst. **124** (2024) 1076. https://doi.org/10.1108/IMDS-08-2023-0581
14 C. Gao, R. Zhang, Q. Tan, Y. Jin, and J. Gao: J. Energy Storage **120** (2025) 116363. https://doi.org/10.1016/j.est.2025.116363
15 C. Yu: Renewable Energy **243** (2025) 122529. https://doi.org/10.1016/j.renene.2025.122529
16 W. Li, M. He, and T. Cai: Energy Rep. **11** (2024) 4222. https://doi.org/10.1016/j.egyr.2024.04.008
17 J. Gao, Q. Meng, J. Liu, and Z. Wang: Renewable Energy **221** (2024) 119806. https://doi.org/10.1016/j.renene.2023.119806
18 C. Yuan, D. Zhao, A. A. Heidari, L. Liu, Y. Chen, and H. Chen: Neurocomputing **607** (2024) 128427. https://doi.org/10.1016/j.neucom.2024.128427
19 M. Abdel-Basset, R. Mohamed, and M. Abouhawwash: Knowledge-Based Syst. **284** (2024) 111257. https://doi.org/10.1016/j.knosys.2023.111257